Viscoelastic shear lag model to predict the micromechanical behavior of tendon under dynamic tensile loading

Jiayu Wu , Hong Yuan , Longyuan Li , Kunjie Fan , Shanguang Qian , Bing Li

PII: S0022-5193(17)30481-2
DOI: 10.1016/j.jtbi.2017.10.018
Reference: YJTBI 9242

To appear in: *Journal of Theoretical Biology*

Received date: 13 July 2017
Revised date: 13 October 2017
Accepted date: 16 October 2017

Please cite this article as: Jiayu Wu , Hong Yuan , Longyuan Li , Kunjie Fan , Shanguang Qian , Bing Li , Viscoelastic shear lag model to predict the micromechanical behavior of tendon under dynamic tensile loading, *Journal of Theoretical Biology* (2017), doi: 10.1016/j.jtbi.2017.10.018

Hightlights

- We explain why the regularly staggering alignment microstructure is frequently selected in natural biological tissues.
- We explore the basic design principles by using the concept of biological tissues.
- The molecular mechanism of tendon rupture can be obtained.
- We give an explicit explanation of why the creep of tendon will cause tendinopathy.
- The failure of tendon is sensitive to loading rate.

Viscoelastic shear lag model to predict the micromechanical behavior of tendon under dynamic tensile loading

Jiayu Wu[a,b], Hong Yuan[a,*], Longyuan Li[b], Kunjie Fan[b], Shanguang Qian[c], Bing Li[d]
[a]MOE Key Laboratory of Disaster Forecast and Control in Engineering, Institute of Applied Mechanics, Jinan University, Guangzhou 510632, China
[b]School of Engineering, University of Plymouth, Drake Circus, Plymouth PL4 8AA, UK
[c]Architecture Engineering Faculty, Kunming Metallurgy College, Kumming 650033, China
[d]Blackett Laboratory, Imperial College London, South Kensington Campus, SW7 2AZ, UK

Address correspondence to Hong Yuan, School of Mechanics and Construction Engineering, Jinan University, Guangzhou 510632, China. Electronic mail: tyuanhong@jnu.edu.cn

Abstract: Owing to its viscoelastic nature, tendon exhibits stress rate-dependent breaking and stiffness function. A Kelvin-Voigt viscoelastic shear lag model is proposed to illustrate the micromechanical behavior of the tendon under dynamic tensile conditions. Theoretical closed-form expressions are derived to predict the deformation and stress transfer between fibrils and interfibrillar matrix while tendon is dynamically stretched. The results from the analytical solutions demonstrate that how the fibril overlap length and fibril volume fraction affect the stress transfer and mechanical properties of tendon. We find that the viscoelastic property of interfibrillar matrix mainly results in collagen fibril failure under fast loading rate or creep rupture of tendon. However, discontinuous fibril model and hierarchical structure of tendon ensure relative sliding under slow loading rate, helping dissipate energy and protecting fibril from damage, which may be a key reason why regularly staggering alignment microstructure is widely selected in nature. According to the growth, injury, healing and healed process of tendon observed by many researchers, the conclusions presented in this paper agrees well with the experimental findings. Additionally, the emphasis of this paper is on micromechanical behavior of tendon, whereas this analytical viscoelastic shear lag model can be equally applicable to other soft or hard tissues, owning the similar microstructure.

Keywords: Tendon; Biocomposites; Shear lag model; Kelvin-Voigt viscoelastic model; Mechanical response;

1. Introduction

Tendons are viscoelastic and hierarchical structure that performs the main function of transferring forces from muscles to bones to generate smooth movement (Gatt et al., 2015; Kanazawa et al., 2016; Magnusson et al., 2010; Nourissat et al., 2015), as shown in Fig. 1a. Tendon serves as a buffer due to its intermedia stiffness between that of bone and that of muscle, which is capable to protect bone and muscle from damage effectively (Passerieux et al., 2007). However, tendinopathy has become a major public health issue, affecting one of every ten people and one of every two runners (Gaida et al., 2010). Tendon pathologies range from chronic injury to acute injury with partial or complete tendon rupture (Nourissat et al., 2015). Owing to its viscoelastic behavior, tendon acute injury is responsible for extremely large force or sudden force, such as the Achilles tendon rupture of athlete due to the overexertion (Docheva et al., 2015). Chronic injury results from overusing tendon for a long time even though applied force is small (Kaux et al., 2011), considering the case of the white collar's rotator cuff tears resulting from using computer for very long hours. Notably, tendon injury is not only related to applied force, but also sensitive to loading rate.

Histologically, tendons are composed mostly of dense connective tissue fascicles, which are tightly packed and highly aligned by collagen fibers (Killian et al., 2012; Liu et al., 2008). The nanoscale structured fibrils with parallel arrays combine to form fibers, which are the primary element to bearing tensile loading in tendon surrounded by a non-collagen interfibrillar matrix including fibroblast (Ahmadzadeh et al., 2013). The dominant component of collagen fibril is type I collagen (Screen et al., 2005) (Fig. 1b). The interfibrillar matrix consists of water, proteoglycans, elastin, glycosaminoglycan and cellular material (Fleissner et al., 2016). Determination of tendon's microstructure functional relationship is critical for figuring out how the stresses are transferred between muscle and bone and for understanding the damage in the tissue. Moreover, in order to have a deep and comprehensive understanding of tendon's mechanical properties from macrostructure to microstructure level, micromechanical analysis of tendon makes total sense.

As the fibril is the fundamental element for bearing loading, both collagen fibrils and the surrounding non-collagen interfibrillar matrix play a vital role in stress transfer under tensile loading. Some previous studies have shown that collagen fibrils are continuous along the entire tendon's length so that the stresses are transferred only in the fibrils and the mechanical function mechanism of non-collagen interfibrillar matrix could be ignored (Craig et al., 1989; Provenzano and Vanderby Jr, 2006). On the contrary, several other studies focus on load transfer contributed by interfibrillar matrix (Ahmadzadeh et al., 2013; Redaelli et al., 2003). Some recent studies (Ahmadzadeh et al., 2013; Szczesny and Elliott, 2014a) on the multiscale experimental testing of tendon fascicles indicated that the parallel-aligned fibrils are discontinuous and the shear stresses are transferred between fibrils through interfibrillar matrix. A shear lag model was employed to explicitly illustrate the force transfer between discontinuous fibrils.

The shear lag model was originally proposed by Cox in 1952 (Cox, 1952), which is commonly applied to represent fiber reinforced composite material consisting of discontinuous fibers embedded in a softer matrix as a powerful analytical method for characterizing the mechanical interaction behavior between fibers and matrix (Wu et al., 2015). The model is based on the idealized assumption that the shear stress is transferred at the fiber-matrix interface and the stiffer fiber carries a majority of the normal stress, while the softer matrix is inclined to take the comparatively greater part of the shear strain (Zhao and Ji, 1997). In addition, the modified shear lag models have been also developed for the application of tissues biomechanics (Ahmadzadeh et al., 2014; Ahmadzadeh et al., 2013; Aspden, 1994; Buehler, 2006; Gao et al., 2003; Goh et al., 2007; Jäger and Fratzl, 2000; Szczesny and Elliott, 2014a; Szczesny and Elliott, 2014b; Wei et al., 2012; Zhang et al., 2010). Since tendon has a similar structure to the fiber reinforced composite at microscopic length scale, the formulation of shear lag models with elastic (Ahmadzadeh et al., 2013; Szczesny and Elliott, 2014a), plastic (Szczesny and Elliott, 2014a), elastic-plastic (Szczesny and Elliott, 2014a) interfibrillar matrix have been developed to elucidate the

stress transfer between fibrils in the tendon. However, using the elastic, plastic or elastic-plastic interfibrillar matrix, which instantaneously deforms when a load is applied, tendons deformation is independent of loading rate. Hence the previous models could not give an explicit explanation of why the creep of tendon will cause tendinopathy, such as shoulder pain.

Although numerous studies revealed the mechanical properties of tendons and collagen fibrils, the molecular mechanism of tendon rupture remains poorly understood. Moreover, at microscopic length scale of tendon, regularly staggering of discontinuous fibrils held together by connective interfibrillar matrix in a unidirectional nano biocomposite (see Fig. 1c-1e). The aim of the present study is to explain why the regularly staggering alignment microstructure is frequently selected in nature biological tissues and to explore the basic design principles by using the concept of biological tissues. To investigate the micromechanical properties of tendon, a shear lag model with viscoelastic matrix is constructed to illustrate the deformation and stress transfer in the tendon under dynamic loading conditions. To our knowledge, this is the first time that a viscoelastic shear lag model has been developed to elucidate the micromechanical behavior of the tendon under dynamic tensile conditions, including creep rupture of tendon.

2. Model formulation and solutions

In an attempt to characterize the tendon rupture mainly caused from large force, sudden loading or creep, a Kelvin-Voigt shear lag model is normally used to analyze the stress transfer between collagen fibrils and interfibrillar matrix. Before theoretical derivations of the viscoelastic shear lag model, some assumptions are made as follows:

(i) The elastic modulus of collagen fibril is several orders of magnitude larger than shear modulus of the interfibrillar matrix (Szczesny and Elliott, 2014a) such that the interfibrillar matrix cannot transfer any normal stress between the neighboring fibrils; the stress in the longitudinal direction can only be transferred via shear in interfibrillar matrix.

(ii) The stiffest discontinuous fibrils are surrounded by interstitial fluid and weakest-linked by glycosaminoglycans and proteoglycans, etc., resulting in large deformation and large deformation rate mainly occur in the interfibrillar matrix; all the collagen fibrils are assumed to be linear elastic.

(iii) The distance between adjacent fibrils is over two orders of magnitude smaller than its overlapping length L such that the deformation in tendon is essentially the longitudinal dimensional.

(iv) The neighboring fibrils are parallel aligned along x direction and overlap nearly half of their length along the longitudinal direction regularly (Fig. 2a).

It was reported that the tendon has viscoelastic material behavior (Ganghoffer et al., 2016; Puxkandl et al., 2002; Reuvers et al., 2011; Svensson et al., 2012). Unlike an elastic material, which instantaneously deforms when a load is applied, tendons slowly displace until their equilibrium deformation is reached. A Kelvin-Voigt viscoelastic model (Bower, 2009) containing a spring with shear stiffness G and in parallel with a dashpot with viscosity η (Fig. 2d) is applied for interfibrillar matrix in an attempt to characterize the mechanical response of tendon to dynamic tensile loading according to *in situ* tensile testing and synchrotron X-ray diffraction experiments on rat-tail tendons (Puxkandl et al., 2002),

$$\tau = G\gamma + \eta \frac{\partial \gamma}{\partial t} \tag{1}$$

where G and η are the shear modulus and viscosity coefficient of the interfibrillar matrix, respectively. Though many complicated constitutive relations have been developed by considering the component of the interfibrillar matrix (Ahmadzadeh et al., 2013; Ciarletta and Ben Amar, 2009; Fessel and Snedeker, 2011; Goh et al., 2007; Redaelli et al., 2003; Shen et al., 2011; Zhang et al., 2010), Eq. 1 characterizes the basic stress-strain relation underlying viscoelastic matrix shear lag model. The parameters used in this viscoelastic shear lag model are list in Table 1. A Cartesian coordinate system is placed at the midpoint of a fibril, in such a way that the length direction of fibrils is along x-axis, as shown in Fig. 2b. Interfibrillar matrix shear strain γ can be expressed as follows,

$$\gamma = \frac{u_1(x,t) - u_2(x,t)}{h} \tag{2}$$

where h is the surface-to-surface distance between adjacent fibrils. As the tendon is under loading, stress is transferred from one fibril to the adjacent fibrils through interfibrillar matrix, which is subjected to shear stress and leads to relative sliding between fibrils. δ denotes the relative sliding between adjacent fibrils, which can be expressed as

$$\delta(x,t) = u_1(x,t) - u_2(x,t) \tag{3}$$

The unit cell (Fig. 2b) and infinitesimal body (Fig. 2c) show the two adjacent fibrils, indeed, each fibril are affected by four adjacent fibrils. A shear stress $\tau(x,t)$ acts over the entire fibril circumference, resulting in the equilibrium equations as follows (Szczesny and Elliott, 2014a)

$$\frac{\partial \sigma_1(x,t)}{\partial x} = \frac{2\tau(x,t)}{r} \tag{4}$$

$$-\frac{\partial \sigma_2(x,t)}{\partial x} = \frac{2\tau(x,t)}{r} \tag{5}$$

where r is the radius of the fibrils, σ_1 and σ_2 are the normal stresses of the fibrils, which can be expressed as follows,

$$\sigma_1(x,t) = E_f \varepsilon_1 = E_f \frac{\partial u_1(x,t)}{\partial x}, \quad \sigma_2(x,t) = E_f \varepsilon_2 = E_f \frac{\partial u_2(x,t)}{\partial x} \tag{6}$$

where E_f is the Young's modulus of the fibrils; ε_1 and ε_2 are the normal strains of fibrils. Furthermore, at any point x along fibrils length direction, normal stresses acting on the cross section should maintain their mechanical balance with the loading force $F(t)$, leading to the following equation

$$\sigma_1(x,t)\pi r^2 + \sigma_2(x,t)\pi r^2 = F(x,t) \tag{7}$$

Letting

$$\zeta^2 = \frac{\eta}{G}, L_C = \sqrt{\frac{E_f r h}{4G}} \tag{8}$$

and combining Eqs. 1-8, the partial differential equation (PDE) for relative sliding δ can be obtained

$$\frac{\partial \delta}{\partial t} = \frac{L_C^2}{\zeta^2}\frac{\partial^2 \delta}{\partial x^2} - \frac{1}{\zeta^2}\delta \tag{9}$$

The fibril normal stress σ_1 along the x-direction can be expressed as

$$\sigma_1 = \frac{1}{2}E_f \frac{\partial \delta}{\partial x} + \frac{1}{2}\frac{F}{\pi r^2} \tag{10}$$

with boundary conditions $\sigma_1(0,t)=0$, $\sigma_1(L,t)= F(t)/\pi r^2$. According to Eq. 10, boundary conditions (BCs) can be also written as

$$\frac{\partial \delta(0,t)}{\partial x} = -\frac{F(t)}{E_f \pi r^2}, \quad \frac{\partial \delta(L,t)}{\partial x} = \frac{F(t)}{E_f \pi r^2} \tag{11}$$

and initial condition (IC)

$$\delta(x,0) = \varphi(x) \tag{12}$$

where L_C is the characteristic length over which the stresses are transferred between interfibrillar matrix and fibrils.

A theoretical solution will be employed to solve $\delta(x)$, with the details given in Appendix A. Relative sliding can be derived from solving the nonhomogeneous PDE (Eq. 9) with nonhomogeneous BCs (Eq. 11) and initial condition (Eq. 12).

$$\delta(x,t) = \left[C_0 + D_0(t)\right]e^{-\frac{1}{\zeta^2}t} + \sum_{n=1}^{\infty}\left[C_n + D_n(t)\right]e^{-\left(\frac{1}{\zeta^2}+\frac{L_C^2}{\zeta^2}\frac{n^2\pi^2}{L^2}\right)t}\cos\frac{n\pi x}{L} + \frac{F(t)}{E_f \pi r^2 L}x^2 - \frac{F(t)}{E_f \pi r^2}x \tag{13}$$

Relevant parameters are shown in Appendix A. It can be seen from the Eq. 13 and Appendix A that, C_0 and C_n are determined by the initial condition of relative sliding. If no relative sliding in the beginning,

C_0=C_n=0. D_0 and D_n are resulted from the force applied at the midpoint of fibril.

After the solution of relative sliding is obtained, the expressions for interfibrillar matrix shear stress and normal stress distribution in the fibril can be obtained

$$\sigma_1(x,t)=\sigma_2(x-L,t)=-\frac{n\pi}{2L}\sum_{n=1}^{\infty}\left[C_n+D_n(t)\right]e^{-\left(\frac{1}{\zeta^2}+\frac{L_C^2}{\zeta^2}\frac{n^2\pi^2}{L^2}\right)t}\sin\frac{n\pi x}{L}+\frac{2F(t)}{\pi r^2 L}x-\frac{F(t)}{2\pi r^2} \tag{14}$$

$$\tau(x,t)=-\frac{n^2\pi^2 r}{4L^2}\sum_{n=1}^{\infty}\left[C_n+D_n(t)\right]e^{-\left(\frac{1}{\zeta^2}+\frac{L_C^2}{\zeta^2}\frac{n^2\pi^2}{L^2}\right)t}\cos\frac{n\pi x}{L}+\frac{F(t)}{\pi rL} \tag{15}$$

This indicates that the theoretical solution of fibrils' displacement u_i (i=1, 2), normal stresses σ_i (i=1, 2) and strains ε_i (i=1, 2), and shear stress can be derived if the initial condition and boundary conditions are known.

The macroscale tissue mechanical behavior can be obtained from the micromechanical analysis. For example, the Young's modulus of the material can be predicted by the ratio of the average fibril force over the cross sectional area and the average strain $u_1(L,t)/L$, as follows

$$E(t)=\frac{c_f L\sigma_1(L,t)}{2u_1(L,t)} \tag{16}$$

where c_f is the fibril volume fraction, which is related to the fibril radius r and the distance between adjacent fibril surfaces h (Fig. 2e). The geometric relationship is given by

$$\frac{h}{r}=\sqrt{\frac{\pi}{c_f}}-2 \tag{17}$$

3. Related experiments and parameters

According to governing equation (Eq. 9), the mechanical interaction behavior of tendon depends on two parameters, namely $(L_C/\zeta)^2$ and $1/\zeta^2$, of which the boundary conditions are independent. Actually, the values of these two parameters are determined by the material and geometrical parameters of the tendon apart from the overlap length L (Eq. 8). Note that the initial condition and boundary conditions are independent of these two parameters. Indeed, the boundary conditions depend on the overlap length L and the force applied at the midpoint of fibril $F(t)$. Therefore, the mechanical properties of tendon are determined by fibril effective stiffness, fibril geometrical dimension and the strength of interfibrillar matrix between fibrils, which agrees well with the ultrastructural point of view proposed by Birk et al. (Birk et al., 1997).

3.1. Geometrical parameters

Generally, the fibril length and diameter are different at different growth stages. The length and diameter of relative mature and mature fibrils are larger than those of early fibrils (Birk et al., 1990; Birk et al., 1995; Redaelli et al., 2003). The fibril diameters were measured by researchers using electron microscopy. Three different groups of fibrils were found in adult human tendons; the thinner, mean and thicker fibrils diameter are 10 nm, 40-80 nm and 150-200 nm, respectively (Dyer and Enna, 1976). Similar experimental results were reported by Svensson, who measured mature Achilles tendons diameter ranging from 150-250 nm for thicker fibrils and 50-80 nm for thinner ones (Svensson et al., 1999). Morphometric analysis of thousands of Achilles tendon fibrils showed that the diameters of collagen fibrils are 122-157 nm, and the smallest size class includes fibrils 18-50 nm in diameter. Watanabe et al. showed that the diameter of thinner fibrils is <100 nm in the region of the myotendinous junction, while the diameter of thicker fibrils in the region of the osteotendinous junction is >200 nm (Watanabe et al., 2012). According to the transmission electron microscopy image of

typical cross section through tendon fascicle, fibril volume fraction is approximately in the range of 50% to 70% (Birk et al., 1990; Craig et al., 1989; Dyer and Enna, 1976; Fessel and Snedeker, 2011; Komatsu et al., 2016; Screen et al., 2005; Svensson et al., 1999). Furthermore, Watanabe et al. measured the fibril center-to-center distance in myotendinous junction, middle metacarpal and osteotendinous junction regions, which are 82.14 ± 9.2 nm, 84.18 ± 4.1 nm and 119.79 ± 6.19 nm, respectively (Watanabe et al., 2012). Additionally, fibril surface-to surface distance in myotendinous junction, middle metacarpal and osteotendinous junction regions are also observed in the scanning electron microscope, which are 14.59 ± 0.9 nm, 13.59 ± 1.7 nm and 13.23 ± 0.7 nm, respectively (Watanabe et al., 2012).

Brik et al. investigated the chicken embryo fibril lengths for 12-16 days and found they were in the range from 6 to 95 mm (Birk et al., 1995). Graham et al. reported the chicken embryo fibrils lengths for 12 days and 18 days were 1-51 mm and 3-86 mm, respectively (Graham et al., 2000). Maximum length of rat tail fibrils was found to be 500 μm, which has been used in the finite element simulation of the stress transfer in tendon (Fessel and Snedeker, 2011). From literatures (Provenzano and Vanderby Jr, 2006; Redaelli et al., 2003), it is evident that the fibril length varies from a few micrometers to tens of millimeters.

3.2. Material parameters

Generally, the Young's modulus of fibrils is characterized by the slope of the stress-strain curve of fibrils. The fibril ultimate tensile strength is defined as the stress value when the fibril breaks. Atomic force microscopy (AFM) made it possible for direct mechanical measurement at the fibrillar level (Shen, 2010; Shen et al., 2011). The Young's modulus and ultimate tensile strength of fibrils were found to be in the range 1-5 GPa and 100-500 MPa, respectively (Craig et al., 1989). The collagen fibrils in bovine Achilles tendon were tested using AFM, revealing Young's modulus ranging from 0.2 to 0.8 GPa (van der Rijt et al., 2006). Type I collagen fibril stress-strain relationship with a slope of 500 MPa was investigated by Eppell et al. in a hydrated state (Eppell et al., 2006). Svensson et al. reported that fibril Young's modulus is 2.8 ± 0.34 GPa in human patellar tendon measured by using AFM (Svensson et al., 2012).

A major component of interfibrillar matrix is the liquid, leading to dramatically small shear modulus of matrix connective to fibrils (Gautieri et al., 2012; Kleiman et al., 1984). The shear modulus of interfibrillar matrix is roughly 0.1 MPa, which was applied for numerical calculation by many researchers (Ahmadzadeh et al., 2015; Elliott, 2003; Hoffman, 1992; Lavagnino et al., 2008; van der Rijt et al., 2006). The shear modulus of cross-linking in the overlap region in a wet environment is 3.4 ± 0.2 MPa, as measured by AFM in micromechanical bending experiments (Yang et al., 2008). Yet Szczesny and Elliott assumed that the value of shear modulus is approximately 1 Pa for elastic and elastoplastic shear lag models (Szczesny and Elliott, 2014a). Interfibrillar matrix connective to fibrils performs both elastic and viscous mechanical behaviors. Collagen fibrils provide the primary elastic strength to tendon while the proteoglycan component is largely responsible for the viscoelastic behaviors (Robinson et al., 2004). The viscosity of proteoglycan estimated from experimental result ranges from 0.25 Pa·s to 0.55 Pa·s (Mow et al., 1984). According to viscosity of single collagen fibril measured by Svensson et al. (Svensson et al., 2010) and Shen et al. (Shen et al., 2011), we can know that collagen fibril is the structural material with high stiffness and low viscosity compared to interfibrillar matrix.

After a comprehensive consideration from references configuration, the geometrical and material parameters of the tendon used in this study are obtained originally from experiments, as list in Table 2.

4. Results

4.1. The process of stress transfer

Although many experiments have been carried out by using AFM to measure the micromechanical properties of tendon (Yang et al., 2012; Yang et al., 2008), few researches explored the effect of loading rate on tendon. As the tendon is under tensile stress, some of the elongation of it is related to relative sliding between fibrils, which were demonstrated by the earlier studies (Folkhard et al., 1987; Mosler et al., 1985). According to the constitutive relation (Eq. 1), shear stress acting on the entire fibril is not only closely relevant to relative sliding, but also influenced by relative sliding rate. A unit cell, subjected to the constant stress rate $\dot{\sigma}$=5.8333 MPa/s, is firstly studied. The 2nd fibril is fixed at the end x=0, and tensile stress is acting on 1st fibril at the other end x=L (refer to Fig. 2b). The distribution of the relative sliding between fibrils, the shear stress in the interfibrillar matrix, the normal stress in the fibril and the displacement at different time are shown in Fig. 3.

It can be noted from Fig. 3 that the values of δ, τ, σ_i and u_i are all continuously increasing, while the applied stress at the end x=L is loading. Both maximum relative sliding and maximum shear stress appear at the both ends, and minimum values occur at the midpoint of the overlap length x=L/2 due to the structural symmetry. According to Eq. 1, it can be identified that the stress rate $\dot{\sigma}$=5.8333 MPa/s applied to fibril is a slow loading rate, as the shape of the curve in Fig. 3a and Fig. 3b are extremely similar. The closer distance to the applied force is, the bigger the normal stress in the 1st fibril is; yet the normal stress in the 2nd fibril is in the opposite condition. Obviously, it can be found that $\sigma_1(L/2,t)$= $\sigma_2(L/2,t)$, referring to Eq. 14 and Fig. 3c.

4.2. Effect of the fibril overlap length on stress transfer

In earlier studies, some researchers believed that fibril volume fraction affects the stress transferring in the tendon in which the fibril overlap length plays a significant role (Craig et al., 1989; McBride et al., 1988). Recently, linear elastic mathematical models and finite element models were developed to investigate how fibril overlap length affects the mechanical behavior of tendon (Ahmadzadeh et al., 2013; Redaelli et al., 2003). In the present study, the shear lag model taking into account the viscoelasticity is constructed in an attempt to elucidate the overlap length effects on deformation and stress distribution (Fig. 4).

When the fibril is stretched by a force with a constant slow stress rate $\dot{\sigma}$=5.8333 MPa/s, the distribution of relative sliding is similar to the shear stress distribution (Fig. 4a), and thus is not provided herein. When the fibril overlap length is small, e.g. L=0.25L_C, the relative movement reaches approximately 570 μm along the entire length, which is about 70% of the fibril overlap length, resulting in the shear stress of ~0.064 MPa acting on the entire fibril . It is observed that, the larger the fibril overlap length, the smaller the shear stress and thus the smaller the relative sliding. When the overlap length is L=8L_C, the sliding movement and corresponding shear stress surrounding the overlap length midpoint are close to zero (see Fig. 4a and Fig. 4c). The normal stress distribution along the shorter fibril is close to linear, which is shown in Fig. 4b. In order to gain a visualized understanding of the differences in stress transfer between the long and short fibrils under slow loading rates, a schematic depicting of deformation and stress distribution is plotted in Fig. 4d.

4.3. Effect of the loading rate on stress transfer

In section 4.1, we have discussed the stress distribution and the deformation of fibrils and interfibrillar matrix when tendon was stretched by different stresses but at an identical stress rate. We are now to examine the stress distribution and deformation under the same stress but at different stress rates, as shown in Fig. 5. While tendon is stretched under a fast stress rate, e.g. $\dot{\sigma}$=10000×5.8333 MPa/s, the

shear stress in the region $0.2< x/L<0.8$ is close to zero and at both ends (x=0 or L) is extremely large even though the relative sliding is small (Fig. 5a and Fig. 5b). The normal stress distribution surrounding the midpoint ($x=L/2$) in the 1st fibril remains constant, which equals to 175 MPa (Fig. 5c). According to Fig. 5d, the fibrils displacement is smaller when the applied stress rate is faster.

The mechanical properties of tendon with various viscosity coefficients or shear modulus can be easily obtained according to the closed-form solution to this problem. In order to clarify the relationship between the applied stress rate and material properties of interfibrillar matrix (shear modulus G and viscosity η), the time and spatial coordinate system is rescaled as $T=\dot{\sigma}t$, $X=x/L$. In a similar manner, variables in the governing equations (Eq. 9) can be rescaled as $\Delta(X,T)=\delta/L$, $\partial\Delta/\partial T=(\partial\delta/\partial t)/(\dot{\sigma}L)$, $\partial^2\Delta/\partial X^2=(\partial^2\delta/\partial x^2)/L$. In terms of the rescale variables, Eq. 9 can be expressed as

$$\frac{\eta}{G}\frac{\partial\sigma}{\partial t}\frac{\partial\Delta}{\partial T}=\frac{L_C^2}{L^2}\frac{\partial^2\Delta}{\partial X^2}-\Delta \tag{18}$$

Eq. 18 shows that the interfibrillar matrix with high viscosity has similar stress distribution and deformation in the tendon when all other parameters remain the same. In contrast, the interfibrillar matrix with high shear modulus has opposite tendency.

4.4. Effective stiffness of tendon

It was reported that the geometrical parameters of fibrils (lengths and radius) influence the elastic modulus of tendon greatly (Ahmadzadeh et al., 2013; Craig et al., 1989; McBride et al., 1988; Redaelli et al., 2003). However, the Young's modulus of tendon is affected by the geometrical parameters differently when loaded at different loading rates, as shown in Fig. 6. When the tendon is loaded with a slow loading rate, the Young's modulus has a linear growth in the whole loading process (Fig. 6a and Fig. 6c). However, when the loading rate is fast, the tendon Young's modulus increases nonlinearly owing to the contribution of viscosity of interfibrillar matrix (Fig. 6b and Fig. 6d). No matter with slow or fast loading rate, tendon effective stiffness with larger fibrils volume fraction will be bigger than that with smaller fibrils volume fraction (Fig. 6c and Fig. 6d). Fig. 6b shows that the effective stiffnesses of tendon with fibril overlap lengths L_C, $2L_C$, $4L_C$, $8L_C$, are very close. Note that the fibril volume fraction c_f contains two cross-sectional geometrical parameters, the fibril radius r and the distance between adjacent fibrils surfaces h, as shown in Eq. 17. Hence, we only discuss the relation between the tendon effective stiffness and the fibril volume fraction here, and so does the relation between the fibril failure and the fibril volume fraction in the next section.

4.5. Fibril failure

The geometrical parameters of fibrils not only influence the effective stiffness of tendon, but also the ultimate strength of fibrils (Redaelli et al., 2003). Of course, the ultimate failure of the tendon is based on the assumptions that the interfibrillar links are permanently engaged in the load transfer mechanism although they can unbind and rebind periodically. Different micromechanical behaviors will be examined under slow and fast loading rates (Fig. 7). Note that fibrils with longer overlap length are more susceptible to failure compared to those with shorter overlap length under the same slow loading rate (Fig. 7a). Increasing the fibril overlap length does not have a critical impact on the failure of relative sliding (Fig. 7b). For tendon with smaller fibril volume fraction, the stress in fibrils is larger and thus the smaller radius and larger surface-to-surface distance fibrils are more prone to failure (Fig. 7c and Fig. 7d).

5. Model validation and discussions

A series of *in situ* and *in vitro* uniaxial tensile tests on tendon fascicle were recently carried out to determine the biomechanical behavior of tendon (Fessel and Snedeker, 2011; Puxkandl et al., 2002; Shen, 2010; Shen et al., 2011; Szczesny and Elliott, 2014a; Szczesny and Elliott, 2014b). *In situ* tensile testing and synchrotron X-ray diffraction experiments on rat-tail tendons were implemented by Puxkandl et al. (Puxkandl et al., 2002) under the applied loading rate ranged from 0.0001 to 0.01 mm s^{-1}. Tendon with viscoelastic nature exhibits strain rate-dependent mechanical properties. A microstructural model was established to elucidate the tendon at a hierarchical level, where fibrils and interfibrillar matrix act as coupled Kelvin viscoelastic systems.

Although scientific researchers have advanced experiment apparatus, such as AFM, transmission electron microscope (TEM) and microelectromechanical systems (MEMS), etc., it's difficult to measure the shear stress distribution in the interfibrillar matrix and normal stress distribution along the fibrils. Generally, stress-strain relations of tendon fascicle is measured by researchers in the tensile experiments (Fessel and Snedeker, 2011; Puxkandl et al., 2002; Shen, 2010; Shen et al., 2011). According to the stress-strain relation of the native rat tail tendon fascicle presented by Fessel and Snedeker (Fessel and Snedeker, 2011), nominal stress-nominal strain curves predicted by our current model agree well with the experimental results (Fessel and Snedeker, 2011); it is also in good agreement with the numerical results calculated by Ahmadzadeh et al. (Ahmadzadeh et al., 2013), as shown in Fig. 8a. Furthermore, Fig. 8b depicts the normal stress distribution along the fibril, which is consistent with the numerical results calculated by Redaelli et al. (Redaelli et al., 2003) and Ahmadzadeh et al. (Ahmadzadeh et al., 2013).

From the multiscale micromechanical theoretical analysis, we can clearly see the reason why the fundamental load-carrying element is selected as discontinuous fibrils embedded in the proteoglycan matrix in biological tissues, instead of continuous long fibrils along tendon length. Despite the ultrastructure of tendon has the advantage of dissipating energy, helping protect bone, muscle and collagen molecules in fibrils, ~30% of general practice consultations for musculoskeletal pain are relevant to tendon disorders (Kaux et al., 2011). Consequently, the biomechanical behaviors of wounded, healing and healed tendon throughout the developmental process have become a field of interests (Docheva et al., 2015; Nourissat et al., 2015; Voleti et al., 2012). Viscoelastic shear lag model gives a good explanation to chronic and acute injuries in tendon, which results from long-period slow loading and sudden large loading, respectively. The viscoelastic nature of tendon is sensitive to loading rate and further manifested in the phenomena of creep.

From the perspective of biomedical engineering, this collagen fibril-interfibrillar matrix dynamics model strongly inclines to become the core of the broader multi-scale model in time and space. As for the time, the expansion of the simulation window from a few seconds to a few years can explain several collagen fibril in the gradual deterioration of the mechanism of time. This can help identify common early markers of tendon pathology and promote early treatment. As for the space, bridging from the molecular level to the whole tendon can explain how the macroscopic forces in tendon injury translate into cell and subcellular depletion. This simple and elegant model may be a significant step for understanding the complex interactions between tendon dynamics, hierarchical structure and mechanical forces.

As larger diameter fibril is more likely to break (Fig. 6c and Fig. 6d), fibril diameter in horse tendon remained abnormally small within 14 months following injury. Particularly, fibrils of diameters in excess of 100 nm, commonly found in normal tendon, were totally absent from the observed distributions in the healing tendon (Williams et al., 1985). Similar phenomenon can be found in rabbit ligament. Frank et al. could not find larger diameter fibrils in the healed ligament after 104 weeks postsurgery (Frank et al., 1997). What's more, some of long fibrils will break up into short pieces during tendon rupture, and it is difficult for its regrowth to long fibril (Evrova et al., 2016). As a result, the ultimate strength and effective stiffness of the injured mouse patellar tendon achieved 48% and

63%, respectively, of uninjured values by 8 weeks (Dyment et al., 2012). It is a miracle that the wounded tendon has mastered the law that long-length and large-diameter fibrils have a negative effect on protecting itself from damage, and refuse to remodel its initial state in the healing and healed process (Docheva et al., 2015).

Although the viscoelastic shear lag model provides closed-form solutions for key parameters of tendon micromechanics, the current study is not without limitations. The Kelvin-Voigt model used to model the matrix is reasonable for modelling creep, but does not accurately predict stress relaxation. Another limitation is that only uniformly arranged microstructure has been explored in our study. Practically, random staggering alignment fibrils are widely observed by researchers (Gautieri et al., 2012). When tendon is stretched, the distance between adjacent fibrils surfaces remain unchanged (referring to Eq. 2), leading the analytical method to be more accurate in analyzing small deformation problems. Future extension of this model should be considered the change of distance between adjacent fibrils surface under tensile loading. We hope to address these extensions of our model in the future publications, which may give a micromechanical explanation on the hot topic—negative and large Poisson's ratio (Ahmadzadeh et al., 2015; Gatt et al., 2015).

While the emphasis of the present study is on the micromechanical behavior of tendon, this analytical viscoelastic shear lag model is equally applicable to other soft tissue (ligament, muscle, axon, etc.) possessing the similar hierarchical microstructure. Furthermore, this theoretical method can be also used to explain the deformation and stress transfer in the hard tissue (bone, tooth, etc.) with approximately zero viscosity in the governing equation (Eq. 9). Nevertheless, what we discussed above is about biomaterials, yet this theoretical method has provided great insight into the design of materials that can achieve an outstanding balance of stiffness, strength and ductility (Espinosa et al., 2012; Koyama et al., 2017; Wei et al., 2012).

6. Conclusions

The objective of this study is to explore the molecular mechanism of tendon rupture and the reason why the regularly staggering alignment microstructure is frequently selected in nature biological tissues, such as bone (Jäger and Fratzl, 2000), shell (Kamat et al., 2000; Menig et al., 2000), tooth (Tesch et al., 2001), axon (Ahmadzadeh et al., 2014; Shamloo et al., 2015), platelet (Zhang et al., 2010), etc. As for bone, shell, and teeth, viscosity can be neglected during micromechanical analysis. However, viscosity is a non-negligible physical attribute for soft tissue (Babaei et al., 2017), which may have a great effect on the micromechanical properties of biological tissues. Tendon, a hierarchical structure, is composed of regularly staggering alignment collagen fibrils connected by viscoelastic interfibrillar matrix. Hence, a Kelvin-Voigt viscoelastic shear lag model has been developed to illustrate the micromechanical behavior between collagen fibrils and interfibrillar matrix in the tendon under dynamic loading. Furthermore, a theoretical closed-form solution has been presented to predict the deformation and stress transfer while tendon is stretched. On the basis of the recent experiments (Fessel and Snedeker, 2011; Puxkandl et al., 2002; Redaelli et al., 2003; Reuvers et al., 2011; Shen, 2010; Szczesny and Elliott, 2014a; Szczesny and Elliott, 2014b) and the results presented in this paper, the following conclusions can be drawn:

(1) The maximum shear stress (maximum relative sliding) of interfibrillar matrix appears at both ends of the fibril overlap length; and the minimum shear stress (minimum relative sliding) is at the center. The maximum and minimum normal stresses of collagen fibril are at the midpoint and both ends of the entire fibril length, respectively.

(2) Under the same slow loading rate, interfibrillar matrix with short fibrils bears large shear stress, leading to large shear deformation. On the other hand, the long fibril carries large load, which is located at the midpoint of the entire fibril length and resists to the whole deformation in the tendon.

(3) Slower loading rate (lower viscosity of interfibrillar matrix) is more conducive to stress transfer along the fibril length. When applied loading rate is extremely fast (viscosity is very higher), shear

stress will be concentrated at both ends of the fibril overlap length even though the relative sliding is small.

(4) Geometrical dimensions of fibrils and matrix influence the fibril failure and tendon macroscale effective stiffness. Tendon with larger fibril volume fraction (larger fibril radius or smaller distance between adjacent fibrils surfaces) has higher elastic modulus, but the fibrils are more susceptible to failure, which is independent of applied loading rate. Owing to its viscoelastic nature, tendon exhibits a rate-dependent stiffness and failure. Under slow loading rate, the longer the fibrils, the larger the elastic modulus of the tendon, and the smaller the ultimate strength of tendon. When the loading rate is fast enough, the length of fibrils does not have a critical impact on the fibril failure.

Acknowledgements

The authors gratefully acknowledge the financial support provided by the National Science Foundation of China (No. 11032005), the Major Project of Guizhou Province Department of Science and Technology (2014) 6024 and Academician Workstation of Guizhou Province Department of Science and Technology (2015) 4004.

Appendix A

The relative sliding $\delta(x,t)$ are obtained by theoretical derivation via the following steps:

(i) The solution $\delta(x,t)$ is split into two parts $V(x,t)$ and $W(x,t)$

$$\delta(x,t)=V(x,t)+W(x,t) \tag{A1}$$

$W(x,t)$ carries the burden of the nonhomogeneous BCs, so $W(x,t)$ is assumed to satisfy the BCs

$$\frac{\partial W(0,t)}{\partial x}=-\frac{F(t)}{E_f\pi r^2},\ \frac{\partial W(L,t)}{\partial x}=\frac{F(t)}{E_f\pi r^2} \tag{A2}$$

The simplest function is used for $W(x,t)$ is

$$W(x,t)=\frac{F(t)}{E_f\pi r^2 L}x^2-\frac{F(t)}{E_f\pi r^2}x \tag{A3}$$

(ii) Substituting Eqs. A1 and A3 into Eqs. 9-12, we can obtain the nonhomogeneous PDE with homogeneous BCs and nonhomogeneous IC, which can be expressed as

$$\begin{cases}\dfrac{\partial V}{\partial t}=\dfrac{2L_C^2}{\zeta^2}\dfrac{\partial^2 V}{\partial x^2}-\dfrac{1}{\zeta^2}V+H,\ 0<x<L,\ t>0\\ \dfrac{\partial V(0,t)}{\partial x}=\dfrac{\partial V(L,t)}{\partial x}=0,\ t>0\\ V(x,0)=\varphi(x)-\dfrac{F(0)}{E_f\pi r^2 L}x^2-\dfrac{F(0)}{E_f\pi r^2}x,\ 0\le x\le L\end{cases} \tag{A4}$$

where

$$H(x,t)=\frac{1}{\zeta^2 E_f\pi r^2 L}\left[2L_C^2F(t)-F(t)x^2+F(t)Lx-\zeta^2F'(t)x^2+\zeta^2F'(t)Lx\right] \tag{A5}$$

(iii) Eqs. A4 can be divided into the homogeneous PDE $V_1(x,t)$ with nonhomogeneous IC (Eqs. A6) and the nonhomogeneous PDE $V_2(x,t)$ with homogeneous IC (Eqs. A7).

$$\begin{cases} \dfrac{\partial V_1}{\partial t} = \dfrac{L_C^2}{\zeta^2}\dfrac{\partial^2 V_1}{\partial x^2} - \dfrac{1}{\zeta^2}V_1,\ 0 < x < L,\ t > 0 \\ \dfrac{\partial V_1(0,t)}{\partial x} = \dfrac{\partial V_1(L,t)}{\partial x} = 0,\ t > 0 \\ V_1(x,0) = \varphi(x) - \dfrac{F(0)}{E_f \pi r^2 L}x^2 + \dfrac{F(0)}{E_f \pi r^2}x,\ 0 \le x \le L \end{cases} \tag{A6}$$

and

$$\begin{cases} \dfrac{\partial V_2}{\partial t} = \dfrac{L_C^2}{\zeta^2}\dfrac{\partial^2 V_2}{\partial x^2} - \dfrac{1}{\zeta^2}V_2 + H,\ 0 < x < L,\ t > 0 \\ \dfrac{\partial V_2(0,t)}{\partial x} = \dfrac{\partial V_2(L,t)}{\partial x} = 0,\ t > 0 \\ V_2(x,0) = 0,\ 0 \le x \le L \end{cases} \tag{A7}$$

(iv) The theoretical solution to the problem (Eqs. A6) can be derived by the method of separation of variables.

$$V_1(x,t) = C_0 e^{-\frac{1}{\zeta^2}t} + \sum_{n=1}^{\infty} C_n e^{-\left(\frac{1}{\zeta^2} + \frac{L_C^2}{\zeta^2}\frac{n^2\pi^2}{L^2}\right)t} \cos\frac{n\pi x}{L} \tag{A8}$$

where

$$C_0 = \frac{1}{L}\int_0^L \left[\varphi(x) - \frac{F(0)}{E_f \pi r^2 L}x^2 + \frac{F(0)}{E_f \pi r^2}x\right]dx \tag{A9}$$

$$C_n = \frac{2}{L}\int_0^L \left[\varphi(x) - \frac{F(0)}{E_f \pi r^2 L}x^2 + \frac{F(0)}{E_f \pi r^2}x\right]\cos\frac{n\pi x}{L}dx \tag{A10}$$

(v) We propose to solve this problem (Eqs. A10) by the method of eigenfunction expansion via expanding the unknown solution $V_2(x,t)$ and nonhomogeneous term of PDE $H(x,t)$ in a series of the related homogeneous eigenfunctions.

$$V_2(x,t) = D_0(t)e^{-\frac{1}{\zeta^2}t} + \sum_{n=1}^{\infty} D_n(t) e^{-\left(\frac{1}{\zeta^2} + \frac{L_C^2}{\zeta^2}\frac{n^2\pi^2}{L^2}\right)t} \cos\frac{n\pi x}{L} \tag{A11}$$

where

$$D_0(t) = \int_0^t e^{\frac{1}{\zeta^2}s} h_0(s)\,ds \tag{A12}$$

$$D_n(t) = \int_0^t e^{\left(\frac{L_C^2}{\zeta^2}\frac{n^2\pi^2}{L^2} + \frac{1}{\zeta^2}\right)s} h_n(s)\,ds \tag{A13}$$

$$h_0(t) = \frac{1}{L}\int_0^L H(x,t)\,dx \tag{A14}$$

$$h_n(t) = \frac{2}{L}\int_0^L H(x,t)\cos\frac{n\pi x}{L}dx \tag{A15}$$

References

Ahmadzadeh, H., Smith, D. H., Shenoy, V. B., 2014. Viscoelasticity of tau proteins leads to strain rate-dependent breaking of microtubules during axonal stretch injury: predictions from a mathematical model. Biophysical journal 106, 1123-1133.

Ahmadzadeh, H., Connizzo, B. K., Freedman, B. R., Soslowsky, L. J., Shenoy, V. B., 2013. Determining the contribution of glycosaminoglycans to tendon mechanical properties with a modified shear-lag model. Journal of biomechanics 46, 2497-2503.

Ahmadzadeh, H., Freedman, B. R., Connizzo, B. K., Soslowsky, L. J., Shenoy, V. B., 2015.

Micromechanical poroelastic finite element and shear-lag models of tendon predict large strain dependent Poisson's ratios and fluid expulsion under tensile loading. Acta Biomaterialia 22, 83-91, doi:http://dx.doi.org/10.1016/j.actbio.2015.04.035.

Aspden, R., 1994. Fibre reinforcing by collagen in cartilage and soft connective tissues. Proceedings of the Royal Society of London B: Biological Sciences 258, 195-200.

Babaei, B., Velasquez-Mao, A. J., Thomopoulos, S., Elson, E. L., Abramowitch, S. D., Genin, G. M., 2017. Discrete quasi-linear viscoelastic damping analysis of connective tissues, and the biomechanics of stretching. Journal of the Mechanical Behavior of Biomedical Materials 69, 193-202, doi:http://dx.doi.org/10.1016/j.jmbbm.2016.12.013.

Birk, D., Zycband, E., Winkelmann, D., Trelstad, R., 1990. Collagen fibrillogenesis in situ. Discontinuous segmental assembly in extracellular compartments. Annals of the New York Academy of Sciences 580, 176.

Birk, D. E., Nurminskaya, M. V., Zycband, E. I., 1995. Collagen fibrillogenesis in situ: Fibril segments undergo post‐depositional modifications resulting in linear and lateral growth during matrix development. Developmental Dynamics 202, 229-243.

Birk, D. E., Zycband, E. I., Woodruff, S., Winkelmann, D. A., Trelstad, R. L., 1997. Collagen fibrillogenesis in situ: fibril segments become long fibrils as the developing tendon matures. Developmental Dynamics 208, 291-298.

Bower, A. F., 2009. Applied mechanics of solids. CRC press, Boca Raton.

Buehler, M. J., 2006. Nature designs tough collagen: explaining the nanostructure of collagen fibrils. Proceedings of the National Academy of Sciences 103, 12285-12290.

Ciarletta, P., Ben Amar, M., 2009. A finite dissipative theory of temporary interfibrillar bridges in the extracellular matrix of ligaments and tendons. Journal of the Royal Society Interface 6, 909-924, doi:10.1098/rsif.2008.0487.

Cox, H., 1952. The elasticity and strength of paper and other fibrous materials. British journal of applied physics 3, 72.

Craig, A. S., Birtles, M. J., Conway, J. F., Parry, D. A., 1989. An estimate of the mean length of collagen fibrils in rat tail-tendon as a function of age. Connective tissue research 19, 51-62.

Docheva, D., Müller, S. A., Majewski, M., Evans, C. H., 2015. Biologics for tendon repair. Advanced Drug Delivery Reviews 84, 222-239, doi:http://dx.doi.org/10.1016/j.addr.2014.11.015.

Dyer, R. F., Enna, C. D., 1976. Ultrastructural features of adult human tendon. Cell and tissue research 168, 247-259.

Dyment, N. A., Kazemi, N., Aschbacher‐Smith, L. E., Barthelery, N. J., Kenter, K., Gooch, C., Shearn, J. T., Wylie, C., Butler, D. L., 2012. The relationships among spatiotemporal collagen gene expression, histology, and biomechanics following full‐length injury in the murine patellar tendon. Journal of Orthopaedic Research 30, 28-36.

Elliott, D. M., 2003. Effect of fiber orientation and strain rate on the nonlinear uniaxial tensile material properties of tendon. Journal of Biomechanical Engineering 125, 726-731.

Eppell, S. J., Smith, B., Kahn, H., Ballarini, R., 2006. Nano measurements with micro-devices: mechanical properties of hydrated collagen fibrils. Journal of the Royal Society Interface 3, 117-121.

Espinosa, H. D., Filleter, T., Naraghi, M., 2012. Multiscale Experimental Mechanics of Hierarchical Carbon‐Based Materials. Advanced Materials 24, 2805-2823.

Evrova, O., Houska, J., Welti, M., Bonavoglia, E., Calcagni, M., Giovanoli, P., Vogel, V., Buschmann, J., 2016. Bioactive, Elastic, and Biodegradable Emulsion Electrospun DegraPol Tube Delivering PDGF‐BB for Tendon Rupture Repair. Macromolecular bioscience 16, 1048-1063.

Fessel, G., Snedeker, J. G., 2011. Equivalent stiffness after glycosaminoglycan depletion in tendon—an ultra-structural finite element model and corresponding experiments. Journal of theoretical biology 268, 77-83.

Fleissner, F., Bonn, M., Parekh, S. H., 2016. Microscale spatial heterogeneity of protein structural transitions in fibrin matrices. Science Advances 2, e1501778.

Folkhard, W., Mosler, E., Geercken, W., Knörzer, E., Nemetschek-Gansler, H., Nemetschek, T., Koch, M., 1987. Quantitative analysis of the molecular sliding mechanisms in native tendon collagen—time-resolved dynamic studies using synchrotron radiation. International Journal of Biological Macromolecules 9, 169-175.

Frank, C., McDonald, D., Shrive, N., 1997. Collagen fibril diameters in the rabbit medial collateral ligament scar: a longer term assessment. Connective Tissue Research 36, 261-269.

Gaida, J. E., Alfredson, H., Kiss, Z. S., Bass, S. L., Cook, J. L., 2010. Asymptomatic Achilles tendon pathology is associated with a central fat distribution in men and a peripheral fat distribution in women: a cross sectional study of 298 individuals. BMC musculoskeletal disorders 11, 41.

Ganghoffer, J. F., Laurent, C., Maurice, G., Rahouadj, R., Wang, X., 2016. Nonlinear viscous behavior of the tendon's fascicles from the homogenization of viscoelastic collagen fibers. European Journal of Mechanics - A/Solids 59, 265-279, doi:http://dx.doi.org/10.1016/j.euromechsol.2016.04.006.

Gao, H., Ji, B., Jäger, I. L., Arzt, E., Fratzl, P., 2003. Materials become insensitive to flaws at nanoscale: lessons from nature. Proceedings of the national Academy of Sciences 100, 5597-5600.

Gatt, R., Vella Wood, M., Gatt, A., Zarb, F., Formosa, C., Azzopardi, K. M., Casha, A., Agius, T. P., Schembri-Wismayer, P., Attard, L., Chockalingam, N., Grima, J. N., 2015. Negative Poisson's ratios in tendons: An unexpected mechanical response. Acta Biomaterialia 24, 201-208, doi:http://dx.doi.org/10.1016/j.actbio.2015.06.018.

Gautieri, A., Vesentini, S., Redaelli, A., Buehler, M. J., 2012. Viscoelastic properties of model segments of collagen molecules. Matrix Biology 31, 141-149, doi:http://dx.doi.org/10.1016/j.matbio.2011.11.005.

Goh, K. L., Meakin, J. R., Aspden, R. M., Hukins, D. W., 2007. Stress transfer in collagen fibrils reinforcing connective tissues: effects of collagen fibril slenderness and relative stiffness. Journal of theoretical biology 245, 305-311.

Graham, H. K., Holmes, D. F., Watson, R. B., Kadler, K. E., 2000. Identification of collagen fibril fusion during vertebrate tendon morphogenesis. The process relies on unipolar fibrils and is regulated by collagen-proteoglycan interaction. Journal of molecular biology 295, 891-902.

Hoffman, A., 1992. A Composite Mioromechanioal Model for Connective Tissues: Part II—Application to Rat Tail Tendon and Joint Capsule.

Jäger, I., Fratzl, P., 2000. Mineralized collagen fibrils: a mechanical model with a staggered arrangement of mineral particles. Biophysical journal 79, 1737-1746.

Kamat, S., Su, X., Ballarini, R., Heuer, A., 2000. Structural basis for the fracture toughness of the shell of the conch Strombus gigas. Nature 405, 1036-1040.

Kanazawa, T., Gotoh, M., Ohta, K., Honda, H., Ohzono, H., Shimokobe, H., Shiba, N., Nakamura, K.-i., 2016. Histomorphometric and ultrastructural analysis of the tendon-bone interface after rotator cuff repair in a rat model. Scientific Reports 6.

Kaux, J.-F., Forthomme, B., Le Goff, C., Crielaard, J.-M., Croisier, J.-L., 2011. Current opinions on tendinopathy. J Sports Sci Med 10, 238-253.

Killian, M. L., Cavinatto, L., Galatz, L. M., Thomopoulos, S., 2012. The role of mechanobiology in tendon healing. Journal of shoulder and elbow surgery 21, 228-237.

Kleiman, R., Bishop, D., Pindak, R., Taborek, P., 1984. Shear modulus and specific heat of the liquid-crystal blue phases. Physical Review Letters 53, 2137.

Komatsu, I., Wang, J. H. C., Iwasaki, K., Shimizu, T., Okano, T., 2016. The effect of tendon stem/progenitor cell (TSC) sheet on the early tendon healing in a rat Achilles tendon injury model. Acta Biomaterialia 42, 136-146, doi:http://dx.doi.org/10.1016/j.actbio.2016.06.026.

Koyama, M., Zhang, Z., Wang, M., Ponge, D., Raabe, D., Tsuzaki, K., Noguchi, H., Tasan, C. C., 2017. Bone-like crack resistance in hierarchical metastable nanolaminate steels. Science 355, 1055-1057.

Lavagnino, M., Arnoczky, S. P., Kepich, E., Caballero, O., Haut, R. C., 2008. A finite element model predicts the mechanotransduction response of tendon cells to cyclic tensile loading. Biomechanics and modeling in mechanobiology 7, 405-416.

Liu, Y., Ramanath, H., Wang, D.-A., 2008. Tendon tissue engineering using scaffold enhancing strategies. Trends in biotechnology 26, 201-209.

Magnusson, S. P., Langberg, H., Kjaer, M., 2010. The pathogenesis of tendinopathy: balancing the response to loading. Nature Reviews Rheumatology 6, 262-268.

McBride, D. J., Trelstad, R. L., Silver, F. H., 1988. Structural and mechanical assessment of developing chick tendon. International journal of biological macromolecules 10, 194-200.

Menig, R., Meyers, M., Meyers, M., Vecchio, K., 2000. Quasi-static and dynamic mechanical response of Haliotis rufescens (abalone) shells. Acta Materialia 48, 2383-2398.

Mosler, E., Folkhard, W., Knörzer, E., Nemetschek-Gansler, H., Nemetschek, T., Koch, M., 1985. Stress-induced molecular rearrangement in tendon collagen. Journal of molecular biology 182, 589-596.

Mow, V. C., Mak, A. F., Lai, W. M., Rosenberg, L. C., Tang, L. H., 1984. Viscoelastic properties of proteoglycan subunits and aggregates in varying solution concentrations. Journal of Biomechanics 17, 325-38.

Nourissat, G., Berenbaum, F., Duprez, D., 2015. Tendon injury: from biology to tendon repair. Nature Reviews Rheumatology 11, 223-233.

Passerieux, E., Rossignol, R., Letellier, T., Delage, J., 2007. Physical continuity of the perimysium from myofibers to tendons: involvement in lateral force transmission in skeletal muscle. Journal of structural biology 159, 19-28.

Provenzano, P. P., Vanderby Jr, R., 2006. Collagen fibril morphology and organization: Implications for force transmission in ligament and tendon. Matrix Biology 25, 71-84, doi:http://dx.doi.org/10.1016/j.matbio.2005.09.005.

Puxkandl, R., Zizak, I., Paris, O., Keckes, J., Tesch, W., Bernstorff, S., Purslow, P., Fratzl, P., 2002. Viscoelastic properties of collagen: synchrotron radiation investigations and structural model. Philosophical Transactions of the Royal Society of London B: Biological Sciences 357, 191-197.

Redaelli, A., Vesentini, S., Soncini, M., Vena, P., Mantero, S., Montevecchi, F. M., 2003. Possible role of decorin glycosaminoglycans in fibril to fibril force transfer in relative mature tendons—a computational study from molecular to microstructural level. Journal of biomechanics 36, 1555-1569.

Reuvers, J., Thoreson, A. R., Zhao, C., Zhang, L., Jay, G. D., An, K.-N., Warman, M. L., Amadio, P. C., 2011. The mechanical properties of tail tendon fascicles from lubricin knockout, wild type and heterozygous mice. Journal of structural biology 176, 41-45.

Robinson, P. S., Lin, T. W., Reynolds, P. R., Derwin, K. A., Iozzo, R. V., Soslowsky, L. J., 2004. Strain-rate sensitive mechanical properties of tendon fascicles from mice with genetically engineered alterations in collagen and decorin. Journal of Biomechanical Engineering 126, 252-7.

Screen, H. R., Shelton, J. C., Chhaya, V. H., Kayser, M. V., Bader, D. L., Lee, D. A., 2005. The influence of noncollagenous matrix components on the micromechanical environment of tendon fascicles. Annals of biomedical engineering 33, 1090-1099.

Shamloo, A., Manuchehrfar, F., Rafii-Tabar, H., 2015. A viscoelastic model for axonal microtubule rupture. Journal of biomechanics 48, 1241-1247.

Shen, Z. L., 2010. Tensile mechanical properties of isolated collagen fibrils obtained by micro-electromechanical systems technology. Case Western reserve university.

Shen, Zhilei L., Kahn, H., Ballarini, R., Eppell, Steven J., 2011. Viscoelastic Properties of Isolated Collagen Fibrils. Biophysical Journal 100, 3008-3015, doi:http://dx.doi.org/10.1016/j.bpj.2011.04.052.

Starborg, T., Kalson, N. S., Lu, Y., Mironov, A., Cootes, T. F., Holmes, D. F., Kadler, K. E., 2013. Using transmission electron microscopy and 3View to determine collagen fibril size and three-dimensional organization. Nature protocols 8, 1433-1448.

Svensson, L., Aszódi, A., Reinholt, F. P., Fässler, R., Heinegård, D., Oldberg, Å., 1999. Fibromodulin-null mice have abnormal collagen fibrils, tissue organization, and altered lumican deposition in tendon. Journal of Biological Chemistry 274, 9636-9647.

Svensson, R. B., Hassenkam, T., Hansen, P., Magnusson, S. P., 2010. Viscoelastic behavior of discrete human collagen fibrils. Journal of the Mechanical Behavior of Biomedical Materials 3, 112-115.

Svensson, R. B., Hansen, P., Hassenkam, T., Haraldsson, B. T., Aagaard, P., Kovanen, V., Krogsgaard, M., Kjaer, M., Magnusson, S. P., 2012. Mechanical properties of human patellar tendon at the hierarchical levels of tendon and fibril. Journal of applied physiology 112, 419-426.

Szczesny, S. E., Elliott, D. M., 2014a. Incorporating plasticity of the interfibrillar matrix in shear lag models is necessary to replicate the multiscale mechanics of tendon fascicles. Journal of the Mechanical Behavior of Biomedical Materials 40, 325-338, doi:http://dx.doi.org/10.1016/j.jmbbm.2014.09.005.

Szczesny, S. E., Elliott, D. M., 2014b. Interfibrillar shear stress is the loading mechanism of collagen fibrils in tendon. Acta biomaterialia 10, 2582-2590.

Tesch, W., Eidelman, N., Roschger, P., Goldenberg, F., Klaushofer, K., Fratzl, P., 2001. Graded microstructure and mechanical properties of human crown dentin. Calcified Tissue International 69, 147-157.

van der Rijt, J. A., van der Werf, K. O., Bennink, M. L., Dijkstra, P. J., Feijen, J., 2006. Micromechanical testing of individual collagen fibrils. Macromolecular bioscience 6, 697-702.

Veres, S. P., Lee, J. M., 2012. Designed to fail: a novel mode of collagen fibril disruption and its relevance to tissue toughness. Biophysical journal 102, 2876-2884.

Voleti, P. B., Buckley, M. R., Soslowsky, L. J., 2012. Tendon healing: repair and regeneration. Annual review of biomedical engineering 14, 47-71.

Watanabe, T., Imamura, Y., Suzuki, D., Hosaka, Y., Ueda, H., Hiramatsu, K., Takehana, K., 2012. Concerted and adaptive alignment of decorin dermatan sulfate filaments in the graded organization of collagen fibrils in the equine superficial digital flexor tendon. Journal of anatomy 220, 156-163.

Wei, X., Naraghi, M., Espinosa, H. D., 2012. Optimal Length Scales Emerging from Shear Load Transfer in Natural Materials: Application to Carbon-Based Nanocomposite Design. ACS Nano 6, 2333-2344, doi:10.1021/nn204506d.

Williams, I. F., Craig, A. S., Parry, D. A. D., Goodship, A. E., Shah, J., Silver, I. A., 1985. Development of collagen fibril organization and collagen crimp patterns during tendon healing. International

Journal of Biological Macromolecules 7, 275-282, doi:http://dx.doi.org/10.1016/0141-8130(85)90025-X.

Wu, J., Yuan, H., Liu, R., 2015. Theory and calculation of stress transfer between fiber and matrix. Applied Mathematics and Mechanics 36, 815-826.

Yang, L., van der Werf, K. O., Dijkstra, P. J., Feijen, J., Bennink, M. L., 2012. Micromechanical analysis of native and cross-linked collagen type I fibrils supports the existence of microfibrils. Journal of the Mechanical Behavior of Biomedical Materials 6, 148-158, doi:http://dx.doi.org/10.1016/j.jmbbm.2011.11.008.

Yang, L., van der Werf, K. O., Fitié, C. F. C., Bennink, M. L., Dijkstra, P. J., Feijen, J., 2008. Mechanical Properties of Native and Cross-linked Type I Collagen Fibrils. Biophysical Journal 94, 2204-2211, doi:http://dx.doi.org/10.1529/biophysj.107.111013.

Zhang, Z., Liu, B., Huang, Y., Hwang, K., Gao, H., 2010. Mechanical properties of unidirectional nanocomposites with non-uniformly or randomly staggered platelet distribution. Journal of the Mechanics and Physics of Solids 58, 1646-1660.

Zhao, P., Ji, S., 1997. Refinements of shear-lag model and its applications. Tectonophysics 279, 37-53.

Table 1 Symbols used in the viscoelastic shear lag model

Variable	Brief description
E_f	Fibril Young's modulus
G	Interfibrillar matrix shear modulus
η	Interfibrillar matrix viscosity coefficient
L	Half-length of fibril
L_C	Characteristic load transfer length
r	Fibril radius
h	Distance between adjacent fibrils surfaces
δ	Relative displacement between adjacent fibrils
u_i	Displacement of i-th fibril
ε_i	Normal strain of i-th fibril
σ_i	Normal stress of i-th fibril
τ	Interfibrillar matrix shear stress
γ	Interfibrillar matrix shear strain
F	Force at the midpoint of fibril
c_f	Fibril volume fraction

Table 2 Parameter values

Parameter	Value
E_f	0.75-1 GPa
G	0.5-1 Pa
r	75-85 nm
L	50-5000 μm
c_f	0.7
η	0.35 Pa·s
σ_b	350 MPa

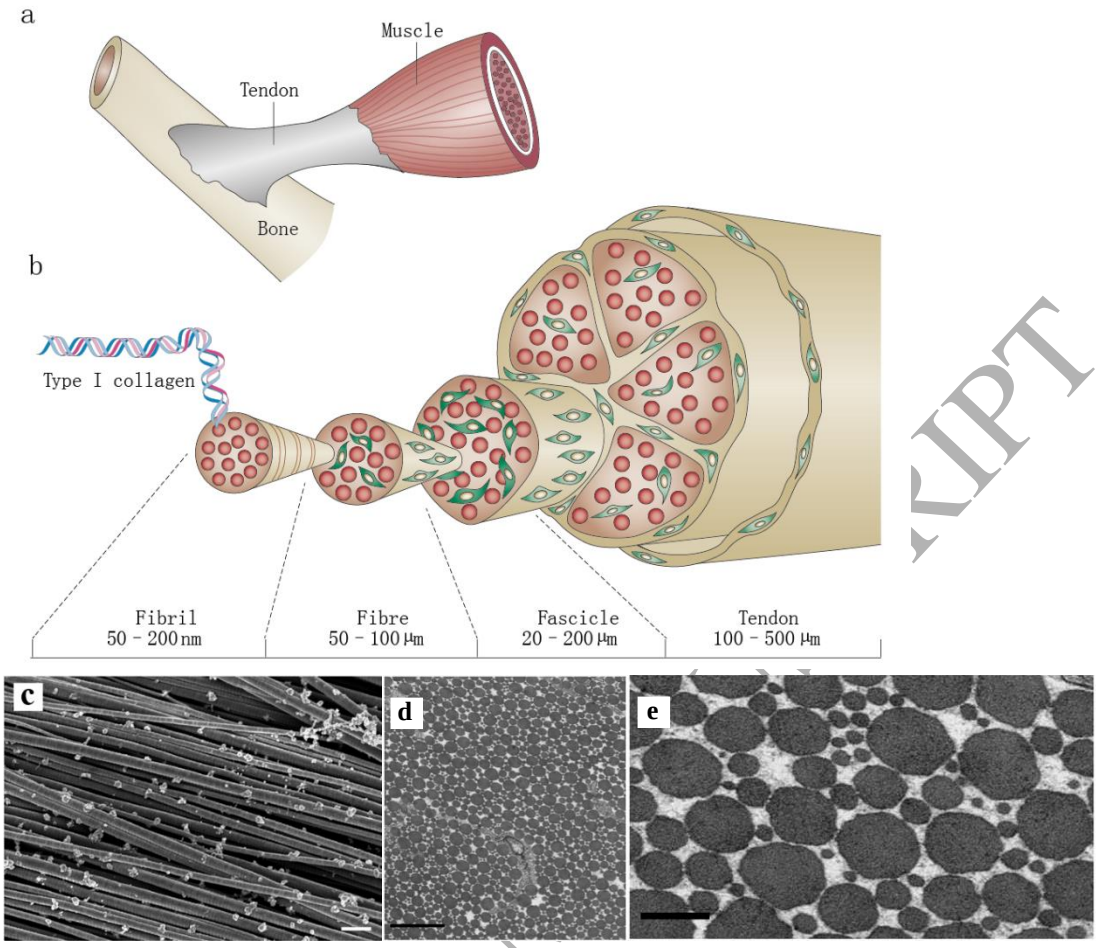

Fig. 1 (a) Tendon connects muscle to bone and plays an important role in transmitting force to produce joint movement. (b) Schematic depicting of tendon hierarchical structure. Reprinted with permission (Nourissat et al., 2015). (c) Fibrils with regular parallel arrays were found in the tendon. Scale bar, 500 nm. Reprinted with permission (Veres and Lee, 2012). (d) Typical cross section through fascicle, showing fibrils. Scale bar, 100 nm. (e) An enlarged view of tendon fibril cross section, roughly a circle. Scale bar, 200 nm. Reprinted with permission (Starborg et al., 2013).

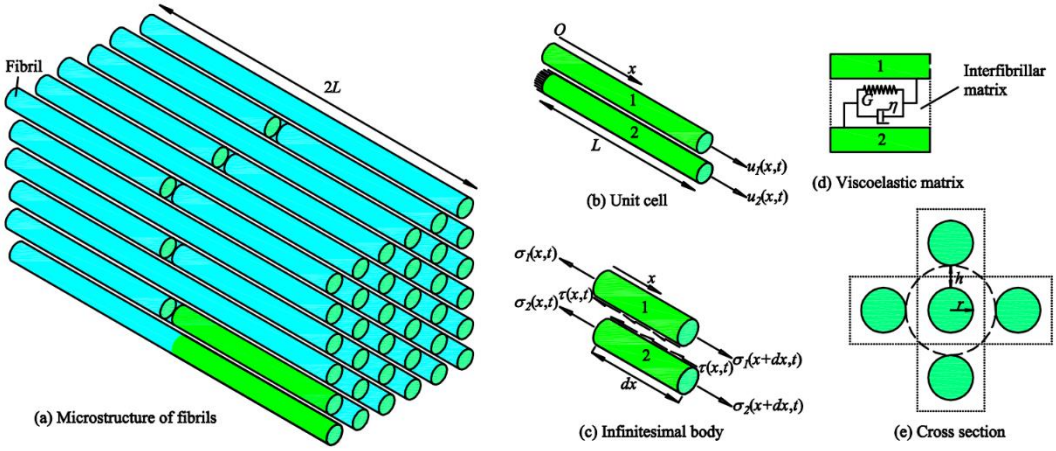

Fig. 2 (a) The microstructure consists of fibrils embedded in an interfibrillar matrix; (b) A unit cell with two adjacent fibrils used in the shear lag model; (c) Equilibrium in infinitesimal body; (d) A Kelvin-Voigt viscoelastic model considered for interfibrillar matrix with a spring and a dashpot; (e) Each fibril is neighboring four fibrils. The central fibril can be considered to be embedded in the cylindrical interfibrillar matrix with the thickness *h*.

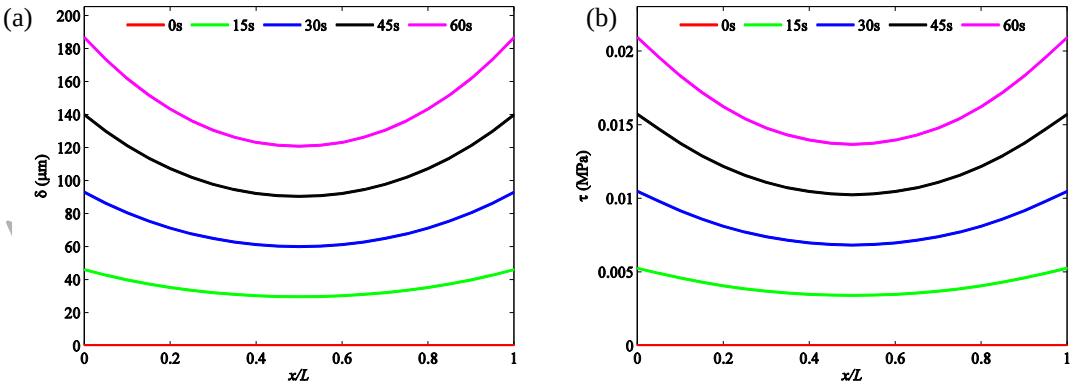

(c) (d)

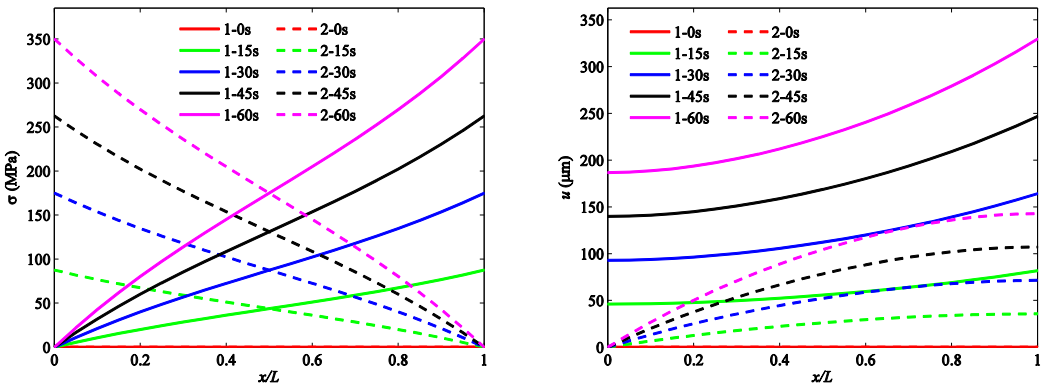

Fig. 3 Distribution of the (a) relative sliding, (b) shear stress, (c) normal stress and (d) displacement along the fibril direction at different times. Solid line and dashed line denote the 1st and 2nd fibrils, respectively. Model parameter used in the calculation are n=30, E_f=1 GPa, r=75 nm, c_f=0.7, G=1 Pa, η=0.35 Pa·s, L=2L_C=816.39 μm, $\dot{\sigma}$=5.8333 MPa/s.

(a)

(b)

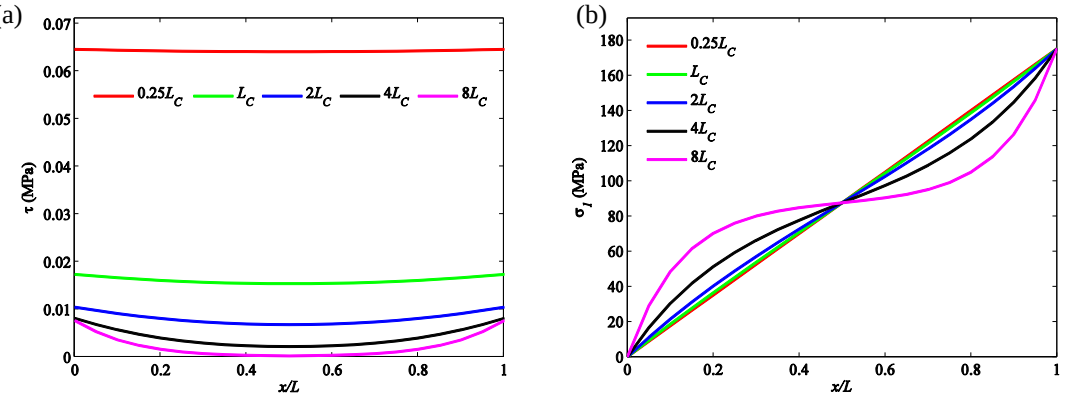

(c)

(d)

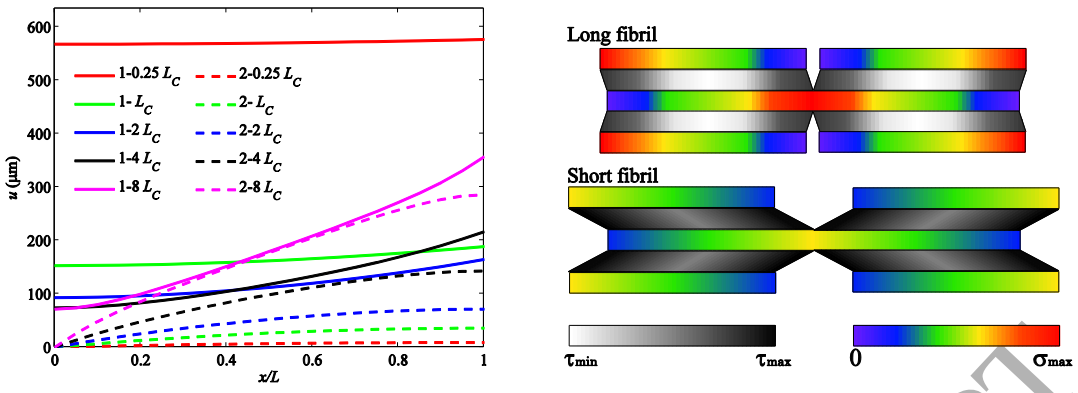

Fig. 4 Distribution of (a) shear stress, (b) normal stress and (c) displacement along the fibril direction at different overlap lengths. Solid line and dashed line denote the 1st and 2nd fibrils. Model parameters used in calculation are n=30, E_f=1 GPa, r=75 nm, c_f=0.7, G=1 Pa, η=0.35 Pa·s, L_C=408.19 μm, $\dot{\sigma}$=5.8333 MPa/s, t=30 s. (d) Schematic depicting of shear stress distribution in interfibrillar matrix and normal stress distribution along fibril when tendon is stretched under the same normal strain.

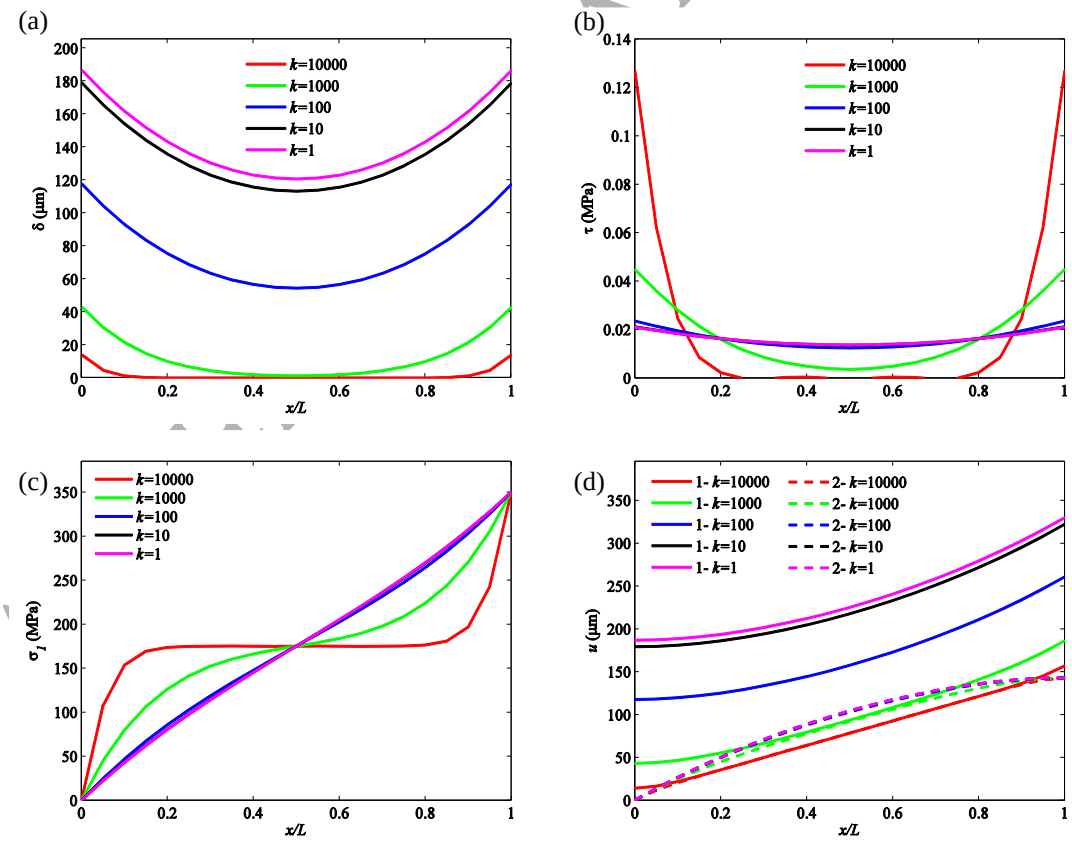

Fig. 5 Distribution of (a) relative sliding, (b) shear stress, (c) normal stress and (d) displacement along fibril direction at different loading rates. Solid line and dashed line denote the 1st and 2nd fibrils. Model parameter used in calculation are n=30, E_f=1 GPa, r=75 nm, c_f=0.7, G=1 Pa, η=0.35 Pa·s, L=2L_C=816.39 μm, $\dot{\sigma}$=k×5.8333 MPa/s, t=60/k s.

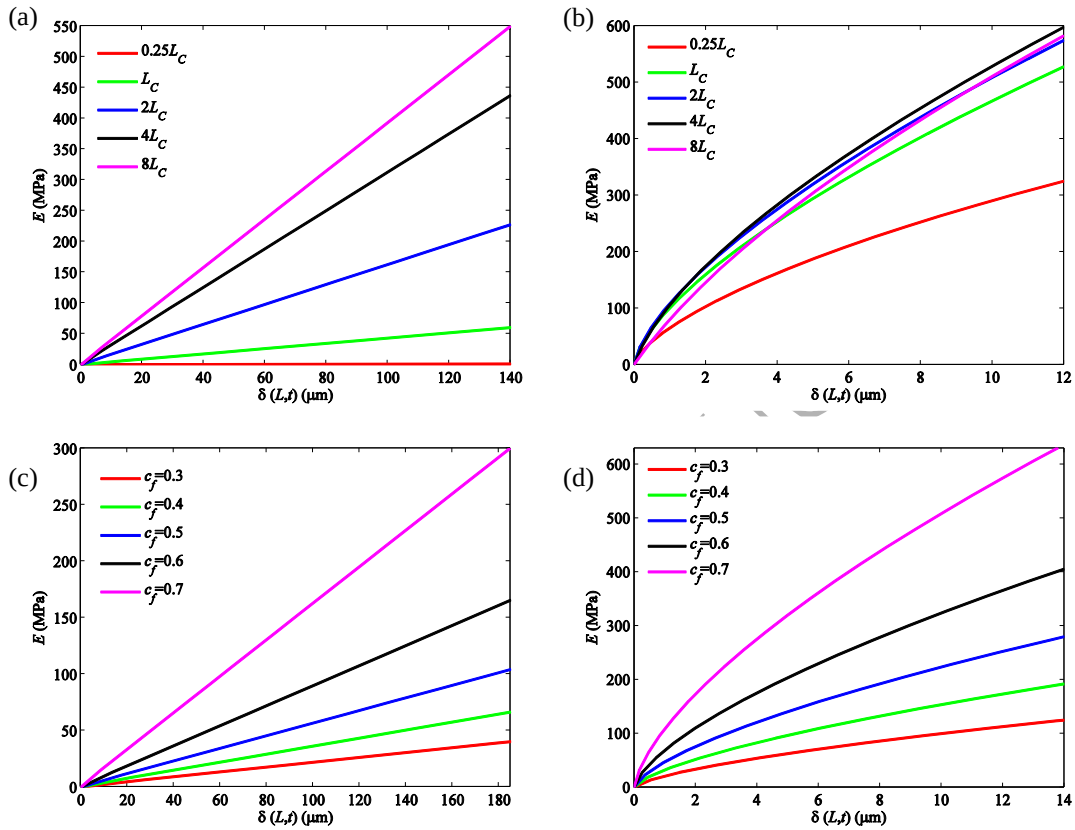

Fig. 6 Plot of Young's modulus over relative sliding (a) with slow loading rate $\dot{\sigma}$=1×5.8333 MPa/s, c_f=0.7; (b) with fast loading rate $\dot{\sigma}$=10000×5.8333 MPa/s, c_f=0.7; (c) with slow loading rate $\dot{\sigma}$=1×5.8333 MPa/s, L=2L_C=816.39 μm; (d) with fast loading rate $\dot{\sigma}$=10000×5.8333 MPa/s, L=2L_C; Other model parameters used in calculation are n=30, E_f=1 GPa, r=75 nm, c_f=0.7, G=1 Pa, η=0.35 Pa·s.

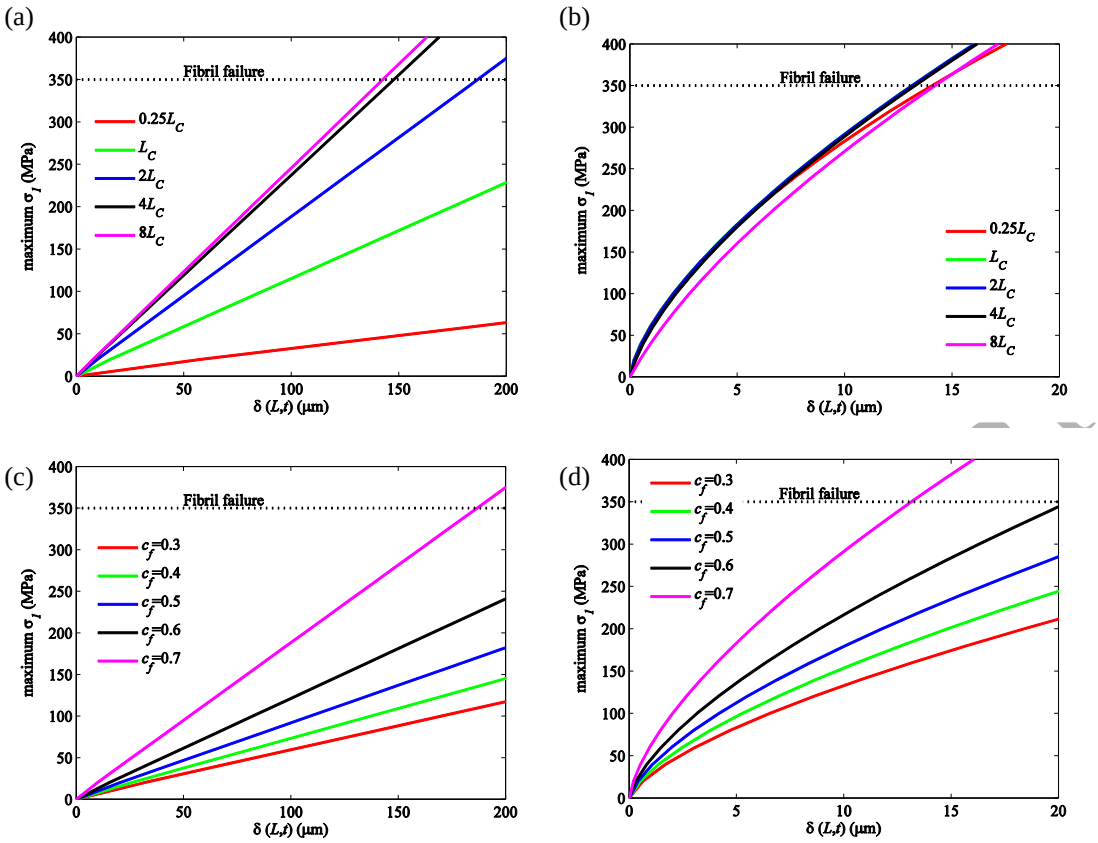

Fig. 7 Plot of maximum normal stress in fibril over relative sliding (a) with slow loading rate $\dot{\sigma}$=1×5.8333 MPa/s, c_f=0.7; (b) with fast loading rate $\dot{\sigma}$=10000×5.8333 MPa/s, c_f=0.7; (c) with slow loading rate $\dot{\sigma}$=1×5.8333 MPa/s, L=2L_C=816.39 μm; (d) with fast loading rate $\dot{\sigma}$=10000×5.8333 MPa/s, L=2L_C; Other model parameter used in calculation are n=30, E_f=1 GPa, r=75 nm, c_f=0.7, G=1 Pa, η=0.35 Pa·s.

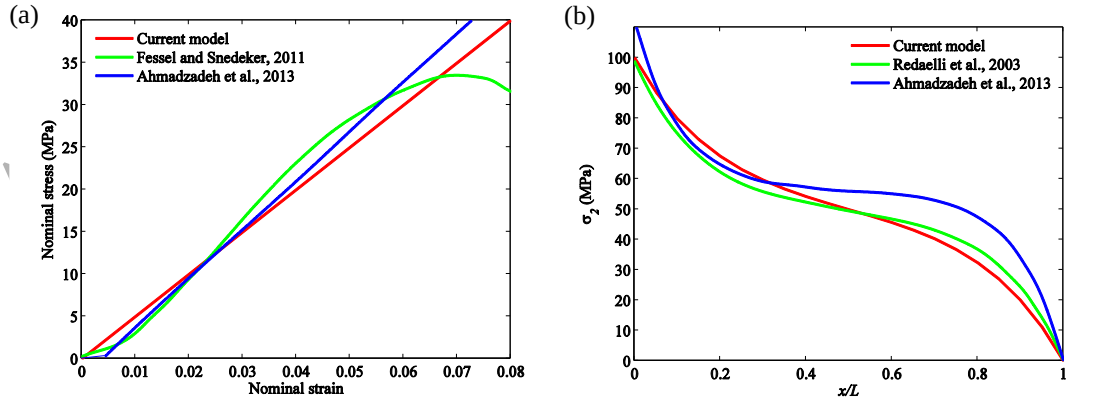

Fig. 8 (a) Nominal stress-nominal strain curve obtained from the present model, experiments (Fessel and Snedeker, 2011) and the model of Ahmadzadeh et al. (Ahmadzadeh et al., 2013). Model parameters used in calculation are n=30, E_f=1 GPa, L=200 μm, r=90 nm, c_f=0.5, G=1 Pa, η=0.35 Pa·s, $\dot{\sigma}$=10 MPa/s, t=60 s. (b) Comparison of normal stress along the fibril between the present model and the

result of Redaelli et al. (Redaelli et al., 2003) and Ahmadzadeh et al. (Ahmadzadeh et al., 2013). Model parameters used in calculation are n=30, E_f=2 GPa, r=90 nm, c_f=0.5, G=1 Pa, η=0.35 Pa·s, $\dot{\sigma}$=1.6667 MPa/s, t=60 s.